A Theoretical Study of the Chemiluminescence of the Al + H_2O Reaction

Sonia Álvarez-Barcia[a,b], Jesús R. Flores[a], Giovanni Granucci[b], Maurizio Persico[b]

[a] Departamento de Química Física, Facultade de Química, Universidade de Vigo, E-36310- Vigo (Spain)

[b] Dipartimento di Chimica e Chimica Industriale, Università di Pisa, I-56126 Pisa (Italy)

Supporting Information.

ABSTRACT: We performed surface hopping simulations of Al + H_2O collisions by a direct semiempirical method, reproducing the conditions of previous beam-gas experiments.[1,2] We observed the formation of the HAlOH species, that dissociates to AlOH + H after a lifetime of about 0.6 ps. This species undergoes nonadiabatic transitions to its first excited state and is responsible for chemiluminescence in the visible range, while the Al-H_2O complex emits in the infrared. The computed emission band in the visible is red shifted with respect to the experimental one,[1,2] because of slight inaccuracies of the potential energy surfaces. However, collisions with more water molecules and exciplex formation with excited Al(^{2}S, ^{4}P) atoms may also contribute to the short wavelength emission, as we show by accurate ab initio calculations.

KEYWORDS. *Reaction Dynamics , Chemiluminescence, Al hydroxides, Surface Hopping*

1 INTRODUCTION

The reaction of Al with water in the gas phase has been the subject of a number of experimental[1,2,3,4,5,6,7] and theoretical studies.[8,9] McClean et al. have studied the kinetics of the title reaction by a laser-induced fluorescence technique, which monitors the decay of Al atoms.[4] Jones and Brewster have employed high-energy conditions and found that the reaction ultimately generates Al_2O_3 particles.[3] Hauge et al.[5] as well as Douglas et al.[7] have performed co-condensation experiments in which HAlOH and AlOH, and perhaps hydrated forms, appear to be formed.[6]

Perhaps one of the most interesting aspects of previous work is the observation that the title reaction is accompanied by a chemiluminescent glow both under single or multiple collision conditions.[1,2] Apart from the general chemical significance of that finding, it had, at the time those works were conducted, the interest of being an explanation to the Al seeding experiments conducted in the upper atmosphere. The authors use a molecular beam apparatus in which a high-temperature thermal beam of Al collides with a tenuous atmosphere of an oxidant, for instance, water, and the emission is recorded. Contrary to other likely oxidants, water appears to produce a chemiluminescent continuum, which is nearly identical to that of the upper atmosphere glows; and that happens both under very low (10^{-5} Torr) or higher pressures (>10^{-3} Torr), which are considered to produce “single” and “multiple” collision conditions.[1] The authors reason that the likely emitter has to be a polyatomic species, otherwise there would be no continuum (but rather, for instance, the characteristic features of excited state AlO or of atomic species). Considering previous theoretical and experimental information, the authors conclude that the emitter should be complex formed by Al and several water molecules or a HAlOH species.[1] However, to our knowledge, there is no new experimental nor any theoretical information about the reaction’s chemiluminescence.

The major product of the gas-phase reaction in its ground state appears to be AlOH + H, which should come mostly from the fragmentation of HAlOH. We have found two competitive mechanisms: [8]

a) $Al + H_2O \rightarrow Al\cdot(H_2O) - [TS12] \rightarrow HAlOH \rightarrow AlOH + H$

b) $Al + H_2O \rightarrow Al\cdot(H_2O) - [TS1H] \rightarrow AlOH + H$

As shown by previous electronic structure studies of the $Al(H_2O)$ system,[10,11,12,13,14,15] $Al\cdot(H_2O)$ is a $Al\text{-}OH_2$ complex,[16,17] which may undergo fragmentation (through TS1H) or hydrogen shift to HAlOH (TS12); those processes have also been found in other atom-water systems.[18,19] We have found that the process (a) is much more important (faster) even at very high T (1000 K).[8] It is interesting to note that the AlOH molecule has recently been detected in the interstellar space,[20] so, in a way, those mechanisms could be of astrophysical importance.

It must also be noted that additional water molecules can have a catalytic effect for they would enable Grotthuss-like molecular mechanisms in the evolution of multi-hydrated complexes, i.e. processes of the type $Al\cdot(H_2O)_n - [TS12_{n-1}] \rightarrow HAlOH\cdot(n\text{-}1)H_2O$.[21,22] Those mechanisms may lower the energy barrier below the level of (ground state) $Al + (H_2O)_n$, which according to previous results, is something which happens for n=2 already. Perhaps it must also be noted that the $HAlOH\cdot(n\text{-}1)H_2O$ and $AlOH\cdot(n\text{-}1)H_2O$ systems ultimately produce higher hydroxides by processes leading to H_2 elimination, which involve neutral intermediates.[21]

As said, the purpose of the present work is to perform the first theoretical study of the chemiluminescence of the gas phase $Al + H_2O$ reaction, by a simulation that mimics as much as possible the experimental conditions.

2 THEORETICAL APPROACH

2.1 General Aspects

The theoretical treatment of the reaction rate for the collision of an uncollimated effusive beam characterized by a temperature T_B and with a stationary gas with temperature T_G reduces to the standard expression for gas mixtures, provided that the relative speed and the averaged cross section is defined by an average temperature T_a, defined as[23]

$$T_a = (m_B T_B + m_G T_G)/(m_B + m_G) \qquad (1)$$

Where m_B and m_G stand for the masses of the beam and stationary gas particles respectively. One is assuming the stationary gas and also the beam are Maxwellian, and also that the gas is isotropic so the result should be independent of the direction of the beam. Moreover, since the beam temperature is much higher than the one of the gas, most non-reactive collisions will slow down the beam atoms. Since we are dealing with activated processes, the possible contribution of those slowed-down atoms should be negligible. Therefore one can restrict the treatment to the first collision of each beam atom, before the thermal equilibration process proceeds. In the end one gets that the bimolecular rate constant can be expressed as

$$k(T_a) = \left(\frac{8 k T_a}{\pi \mu}\right)^{1/2} \sigma_T(T_a) \qquad (2)$$

Here $\sigma_T(T_a)$ is the T-dependent reaction cross section, which relates to the energy-dependent one by:

$$\sigma_T(T_a) = (k T_a)^{-2} \int_0^\infty \sigma(E_r) e^{-E_r/(k T_a)} E_r \, d E_r \qquad (3)$$

where E_r represents the collision energy. The latter cross section relates to the opacity function $P(E_r,b)$ by:

$$\sigma(E_r) = 2\pi \int_0^{b_{max}} P(E_r, b)\, b\, db \qquad (4)$$

where b is the impact parameter. $P(E_r,b)$ represents the reaction probability corresponding to particular values of collision energy and impact parameters.

In a trajectory computation it can be quantified as:[24]

$$P(E_r, b) = N_r(E_r, b)/N_t \qquad (5)$$

Here $N_r(E_r,b)$ and N_t represent the number of reactive trajectories for a particular pair and the total number of trajectories, respectively.

That definition can be extended to processes other than reaction, for instance, photoemission. We could compute the emission probability as:

$$P_{pe}(E_r, b) = N_t^{-1}\left[\sum_{m=1}^{N_t}\left(\sum_{j}^{i(t)-1}\int A_{i(t),j}(t)\,dt\right)_{(m)}\right] \qquad (6)$$

Here $A_{i(t),j}(t)$ represents the Einstein emission coefficient for a $i(t) \rightarrow j$ transition and $i(t)$ is the current electronic state, at time t, for trajectory m. $P_{pe}(E_r,b)$ computed this way is meaningful as long as the emission rate as given by the Einstein coefficient is small in relation with the timescale of the collision event. A differential (frequency specific) probability can be defined as:

$$P_{pe}(E_r, b, [v_a, v_b]) = N_t^{-1}\left[\sum_{m=1}^{N_t}\left(\sum_{j}^{i(t)-1}\int A_{i(t),j}(t; [v_a, v_b])\,dt\right)_{(m)}\right] \qquad (7)$$

Here $A_{i(t),j}(t;[\nu_a,\nu_b])$ is simply $A_{i(t),j}(t)$ but set to zero if the frequency as defined by $(E^{i(t)}-E^{j})/h$ is not within the interval $[\nu_a,\nu_b]$ (i.e. $A_{i(t),j}(t)$ multiplied by a rectangular step function). Using (7) or (6) instead of (5) in expressions (3) and (4) the corresponding E or T dependent cross sections can be computed. The integrals over the impact parameter (4), the collision energies (3) or t (6)-(7) have been computed numerically.

2.2 Nonadiabatic trajectory simulations

We have considered the interaction of Al(^{2}P) with H_2O in its three levels ($^2B_1$,$^2B_2$ and $^2A_1$ for C_{2v} conformations); in other words, we have considered emission from the lowest two excited states into the ground state.

We have performed "on the fly" trajectories with surface hopping (TSH) using the semiempirical Floating Occupation Molecular Orbital Configuration Interaction (FOMO-CI) method.[25,26] The AM1 hamiltonian[27] has been reparameterized to reproduce accurate ab initio data[17] (see the supplementary material for more details).We also applied state-specific and geometry-dependent corrections of the semiempirical PES's, with a procedure that maintains the consistence of electronic energies and wavefunctions (no displacement of PES crossing loci).[28] The optimized semiempirical parameters and the state-specific correction functions can be found in the supplementary material (tables SM_T1 and SM_T2). The method is noted as AM1$^{(*)}$-FOMO-CI.

The (simplified) potential energy surfaces (PES) of the ground and first excited state are depicted schematically in Figure 1. Overall the AM1$^{(*)}$-FOMO-CI method with ad hoc parametrization and PES correction is a reasonable compromise between accuracy and computational speed. It must be noted that, compared to high-level ab initio results (which include scalar relativistic effects),[17] it gives rather good relative energies for M1 and TS12. It underestimates though the depth of the

ground state (^{2}A') M2 well by about 0.20 eV (1600 cm^{-1}). The energy of the M2 minimum for the first excited state relative to the reactants, is in very good agreement with the ab initio reference, but this means that photon emission originating from this geometry (M2*) tends to be displaced to longer wavelengths because the energy gap with the ground state is too small. The main difference between the ground and excited state equilibrium geometries is the H-Al-O angle: 112.7º in X^2A' and 180.0º in 1^2A' (both values still very close to the ab initio ones, 114.8º and 179.4º see ref. 17, figure SM_F1 and table SM_T3 of the supplementary material). The vertical transition energy of M2 (2.62 eV = 21100 cm^{-1}) also agrees very well with the ab initio one (20657 cm^{-1} [17]); in other words, the 1^2A" energy at this geometry is too high by as much as the X^2A' one. We note that this transition energy almost coincides with the main peak in the emission spectrum.

The transition moments vary very much with the geometry; taking the important 1^2A" → X^2A' transition at the equilibrium geometry of M2 as a measure, we have that the AM1$^{(*)}$-FOMO-CI value is 0.7194 a.u. as compared to a relatively high-level ab initio value of 0.8401 a.u.[17] (MRCI/aVTZ//QCISD(T)/6-311++G(2df,p) -multireference configuracion interaction- using a state-averaged CASSCF -complete active space SCF- wavefunction as reference[29,30,31,32,33,34,35,36]). In general, AM1$^{(*)}$-FOMO-CI gives somewhat lower values for the transition moments than MRCI calculations, which would imply that our computed emission cross sections are somewhat underestimated.

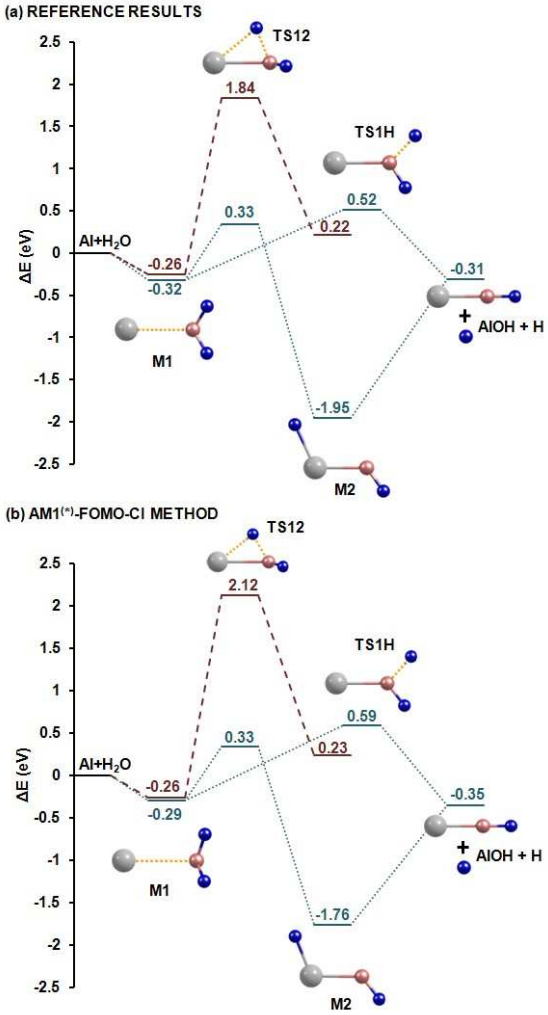

Figure 1. A simplified potential energy surface (PES) of the ground (blue) and first excited state (dark red) (relative energies with respect to Al +H_2O, ZPEs are not included). Reference results include high-level (HL) ab initio values for the ground state (see ref. 17), while for the first excited state we have employed CASSCF/6-311++G**//CASSCF/6-311++G**[33,34,35] energies as follows: relative energies have been computed as $\Delta E_{X^i}^{HL-corr} = \Delta E_X^{HL} + \Delta E_{X^i}^{CASSCF}$ with $\Delta E_{X^i}^{CASSCF} = E_{X^i}^{CASSCF} - E_X^{CASSCF}$, where *X* refers to the structure of interest. Note that the excited state energies are computed on their respective optimized geometries. The MOLPRO 2006 package has been used.[36] (See more details of the structures in the figure SM_F1 and table SM_T3 of the supporting material).

Concerning the initial conditions for the internal energy of water, we have employed a canonical distribution of the rotational energy for *T*=300 K; besides, it has been taken in its vibrational ground state, represented by the normal coordinate approximation and a classical sampling of coordinates

and momenta for the three vibrational degrees of freedom has been applied. On the other hand, we have employed T_a= 860.5 K which corresponds to a beam temperature of 1700 K.

We have run a total of 169200 trajectories in the following way. We have considered a set of 48 collision energies (0< E_r ≤ 2.3 eV) for a number of impact parameters for each energy such that 0 ≤ b ≤ 2.8 Å (see table SM_T4 of the supplementary material). For each energy and impact parameter the trajectories are started at R=10 Å where R is the distance between the center of mass of water and Al; 1/3 of those trajectories are started at each electronic term (which, as said, can be labeled as $^2A_1$, $^2B_1$ and $^2B_2$ for C_{2v} conformations).

The time-dependent Schrödinger equation for the propagation of the electronic wavefunction is solved at each trajectory time step by a local diabatization method, thus providing the state probabilities $P_k(t)$.[25] The variation in time of the $P_k(t)$ probabilities brings about nonadiabatic transitions in the form of surface hopping events, according to Tully's fewest switches algorithm[37] with quantum decoherence corrections.[38] The nonadiabatic dynamics as well as the FOMO-CI method are implemented in a development version of the MOPAC2002 package[39] that has been used throughout this work.

3 RESULTS AND DISCUSSION

3.1 The reaction and photoemission cross sections

Figure 2 displays the computed reaction and total photo-emission cross sections as a function of the collision energy up to 1.2 eV, eventually weighted with the relative energy distribution function as

$$\sigma(E_r,T_a)=(kT_a)^{-2}E_r\sigma(E_r)e^{\frac{-E_r}{kT_a}} \qquad (8)$$

Where $\sigma(E_r,T_a)$ or $\sigma(E_r)$correspond to either the reaction ($\sigma_r(E_r,T_a)$,$\sigma_r(E_r)$) or the photoemission ($\sigma_p(E_r,T_a)$, $\sigma_p(E_r)$¿ processes. Note that (8) corresponds to the integrand of eq. (3). Since both cross sections, $\sigma_r(E_r)$ and $\sigma_p(E_r)$ are very small at low collision energies (E_r < 0.6 eV), the noise to signal ratio of the computed raw data is rather high, in spite of the large number of trajectories. Therefore, we have applied a smoothing procedure by convolution with a Gaussian function of E_r, both in the numerical integration and in the plots of Fig. 2, by replacing $\sigma(E_r)$ with

$$\sigma'(E_r)=\frac{1}{N}\sum_{i=1}^{m}\sigma(E_i)N_i^{1/2}\exp\left(\frac{-(E_r-E_i)^2}{\Delta E^2}\right) \qquad (9)$$

Here $N=\sum_{i=1}^{m}N_i^{1/2}\exp\left(\frac{-(E_r-E_i)^2}{\Delta E^2}\right)$and N_i is the number of trajectories in the batch i, from which the data $\sigma(E_i)$ were obtained. ΔE is an arbitrary width parameter, in this case 0.05 eV.

It is readily seen that the contributions to the temperature dependent cross sections become almost zero for E_r>1 eV, and that is so because of the Boltzmann factor. The computed reaction and total photoemission cross sections are $6.3\cdot10^{-3}$ Å^2 and $2.7\cdot10^{-8}$ Å^2, respectively. The onset of the reaction cross section is at about 0.23 eV, which is, approximately, the energy of the saddle point TS12 relative to the ground state reactants if one includes ZPEs (zero point energies). We have a significant contribution to the emission cross section for lower energies, which comes from M1 and the "entrance channel" (the Al – OH_2 interaction). The rest of the emission comes mostly from M2, that is why it disappears whenever the reaction cross section fades away (E_r >1 eV). It must be noted that tunneling is not taken into account in the present TSH simulations (it is quite difficult in multidi-

mensional computations); however, it should not have a very important impact, especially in the high frequency part of the emission (vide infra), because the tunneling transmission factor is normally close to unity for the effective temperature considered in the present work (T_a= 860.5 K)[17]

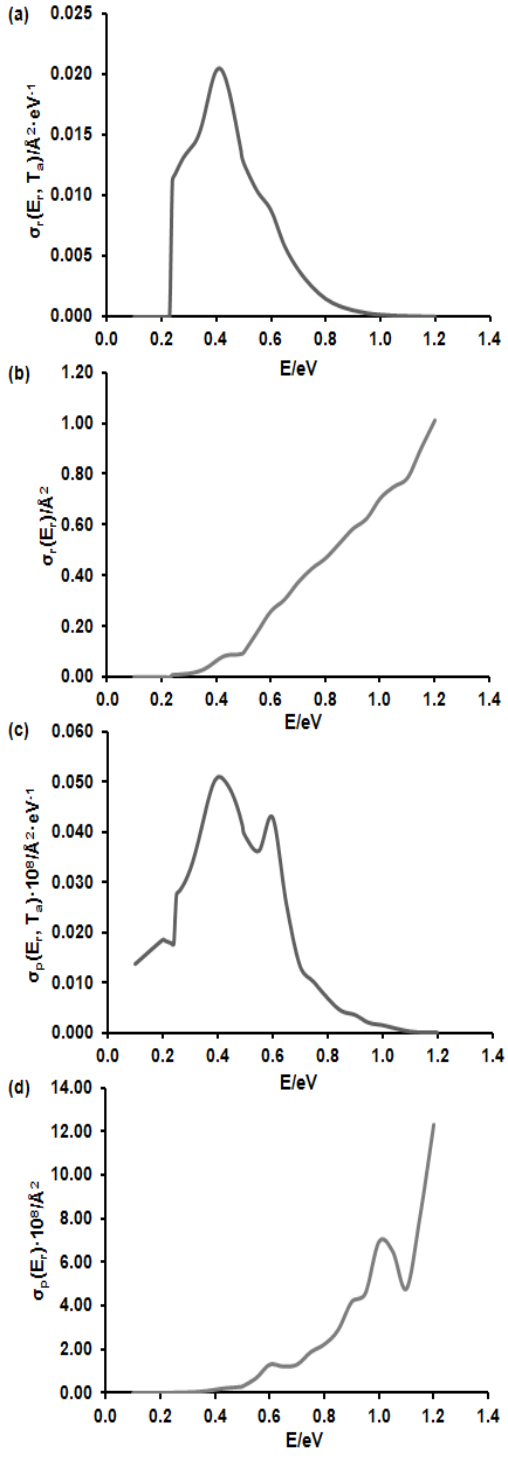

Figure 2. Cross sections as a function of the collision energy.(a) Reaction cross section multiplied by the appropriate Boltzmann factor (see eq. (8)). (b) Reaction cross section without Boltzmann factor. (c) Photoemission cross section multiplied by the Boltzmann factor. (d) Photoemission cross section without Boltzmann factor.

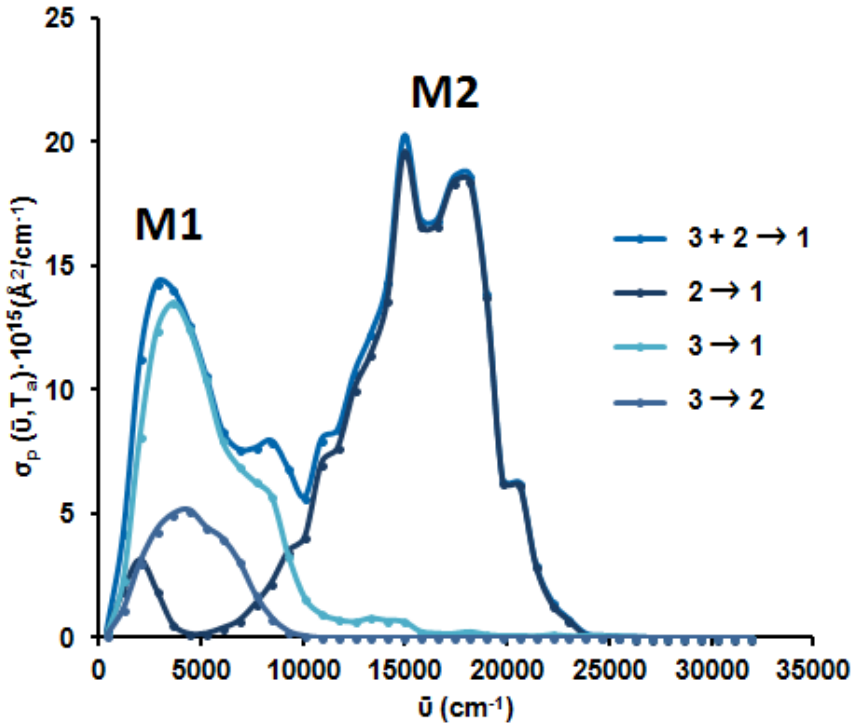

Figure 3. Photoemission cross sections ($Å^2/cm^{-1}$) as a function of the wavenumber (cm^{-1}). 3 and 2 mean the second and first excited states and 1 stands for the ground state.

Figure 3 displays the photoemission cross section as a function of the frequency of the emitted radiation. It is readily seen that we have two bands, one in the infrared, which, as we have verified, corresponds to M1 and the Al-OH_2 collision, and the other starting at approximately 10000 cm^{-1} with maximum intensity in the visible, which corresponds to the emission from, quite specifically, the first excited state of M2. It must be noted that, at the molecular geometry of TS12, the first excited state lies above the ground state by approximately 1.8 eV. As a consequence, in order to ap-

proach the M2 geometry the system must be on the electronic ground state, which is what is actually observed in the trajectories. After that, the trajectories which contribute to the emission probability undergo surface hopping into the first excited state. The system eventually decays into the ground state, frequently after more than one hop back into the excited state. There are typically two or three raids into the excited state, before the system goes into the ground state (see Figure 4) and dissociates to AlOH + H. It turns out the hops occur between the ground and the first excited state where they are quite close in energy, namely at <HAlO angles close to 180º. The emission corresponding to the higher frequencies arises from geometries with a much smaller angle. Note also that there is a conical intersection between the first and the second excited states, which accounts for some population of the latter resulting in very weak emissions to the first excited state (contributing to low frequencies) and to the ground state (higher frequencies). As a matter of fact, emission from the second excited state to the first excited and the ground state has a sizeable impact mostly for M1 and the entrance channel. It is too high in energy to contribute to the emission at the M2 geometry.

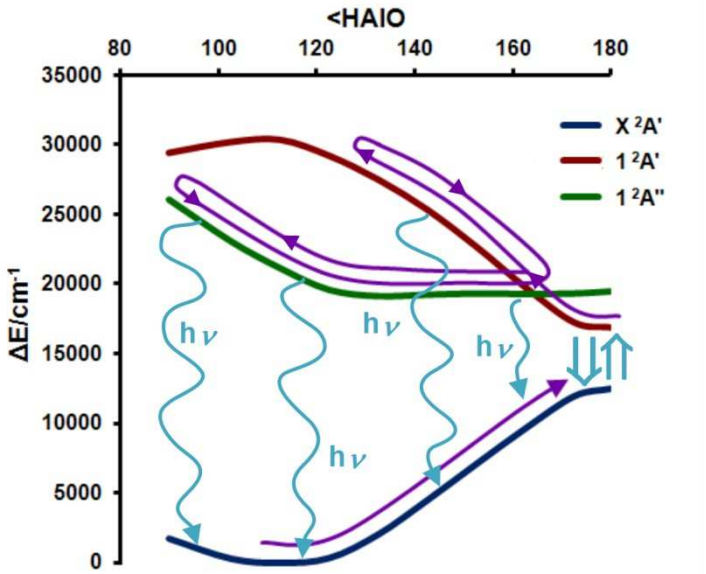

Figure 4. Schematic representation of a typical trajectory contributing to the M2* photoemission probability. The energy profiles are obtained at the AM1$^{(*)}$-FMO-CI level using the frame of the ground state optimized geometry. Hops

occur at conformations with <HAlO angles close to 180º. Recall that the total energy is conserved, while the diagram points to potential energy variations.

It must be noted that the emission recorded in the experiments cannot be caused by (excited state) AlOH or even AlO, for AlOH* and AlO($B^2\Sigma^+$) cannot be formed from Al(X^2P) + H_2O and AlO($A^2\Pi$) would give a band very much shifted to the low-frequency region (see Figure 5). It must be noted that we have not observed AlO formation in the present simulations.

It is also interesting to note that there seem to be two peaks in the visible band of the computed spectrum: one is located at approximately 15000 cm^{-1} and the other at approximately 17500 cm^{-1}. We have found that the low-frequency one arises from accumulation of the emission probability at geometries of the first excited state which are not far to its equilibrium geometry, which happens to be quite close to that of the cis-trans transition structure of the ground state, while the high-frequency one has contributions from emissions taking place at geometries more similar to the M2 (ground state) minimum, where the first excited state is ^{2}A" (for planar geometries).

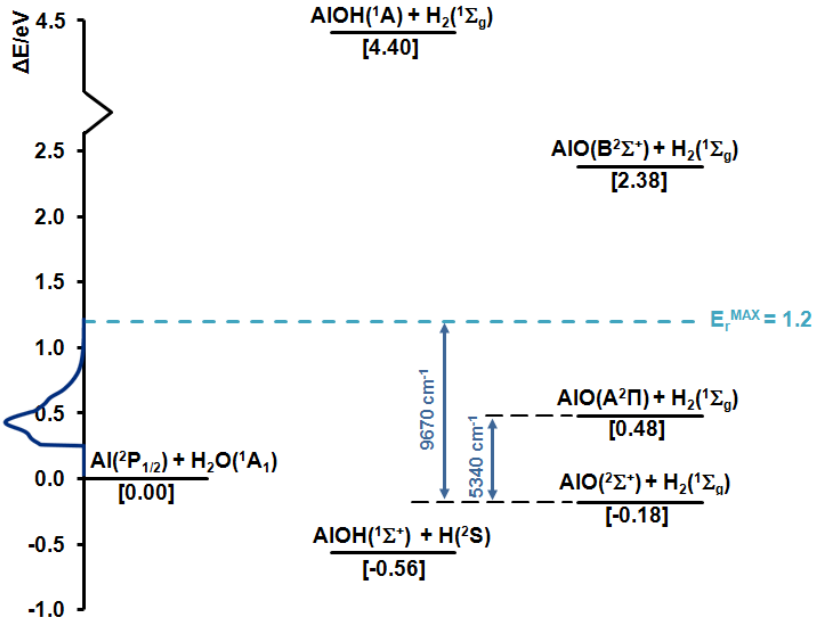

Figure 5. Relative energies (in eV) for the ground state and first excited state of AlO and AlOH species. For the ground state the values are those of a high-level procedure (see reference 17) (ZPE's are included). For the first excited state, the experimental vertical excitation energy tabulated in NIST were added to the ground state value. A schematic curve representing the reaction cross section is given in the *y* axis. Relatives energies (in brackets) are computed with respect to $Al + H_2O$.

In Figure 6 we have displayed the cross section as a function of both the collision energy and the emission frequency. The origin of the peaks of fig. 6 can be traced to the trajectory energy E_r. Again, the very low-frequency (IR) emission comes from non-reactive trajectories. Low-energy reactive trajectories contribute to both the high (17500 cm^{-1}) and the low (15000 cm^{-1}) frequency peaks, while the high-energy range contributes to the high-frequency peak and extends the emission to approximately 23000 cm^{-1}. It must be noted the peaks of the photoemission cross sections are very dependent on T_a, since most of the emission is caused by high-energy trajectories. We have checked that an increase in T_a beyond 860.5 K very much augments the height of the 15000-17500 cm^{-1} peaks, especially as compared to the low-frequency band; however it does not substantially extend the reach of the band to higher wavenumbers.

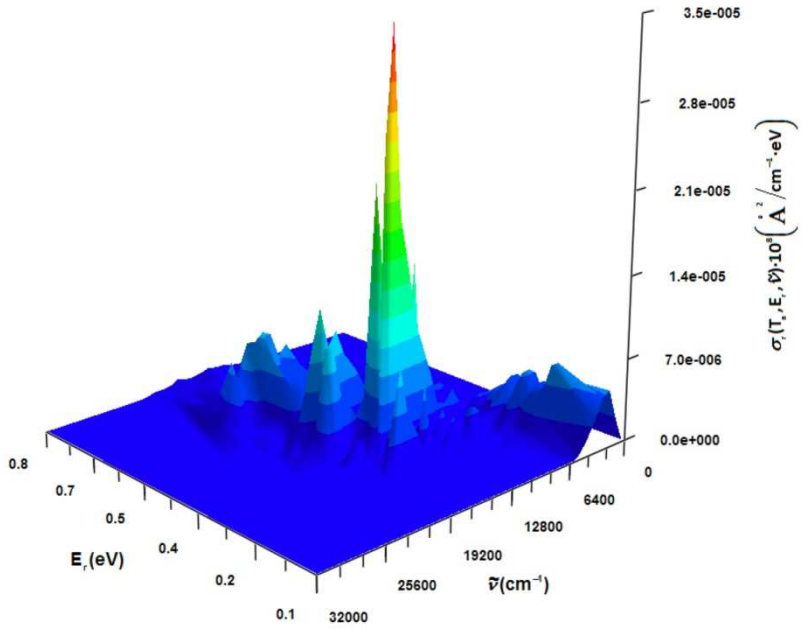

Figure. 6. Wavenumber-dependent photoemission cross section. The values include the Boltzmann factor of eq. (3).

3.2 Comparison to the experiment

The experimental emission is a wide band starting approximately from 3500 Å (28570 cm^{-1} or 3.5 eV), with a weak tail at long wavelengths that was recorded up to 8200 Å (12200 cm^{-1} or 1.5 eV).[1,2] The short wavelength band is the most unsatisfactory feature of the computed emission spectrum (fig. 3), for the experimental spectrum[1,2] extends well into about 29000 cm^{-1}, the maximum appearing at about 22000 cm^{-1}. Part of the difference comes from the fact that, at the ground state geometry of M2, both the X^2A' and $1^2A''$ state energies are overestimated (less deep with respect to Al + H_2O) by roughly 0.20 eV (X^2A' by 1550 cm^{-1} and $1^2A''$ by 1900 cm^{-1}). As a consequence, after hopping to the excited state at large H-Al-O angles, the system finds a steep slope (steeper than the ab initio calculations do suggest) along the H-Al-O bending coordinate, i.e. the geometry deformation leading to larger X^2A'-$1^2A''$ energy gaps. This fact may explain why the high frequency emission region is reached less frequently in our simulations. The limitations of the TSH treatment with respect to quantum wavepacket dynamics (no tunneling, energy conservation imposed to each trajectory af-

ter a surface hopping) may also contribute to decrease the probability of climbing to high potential energies in the excited state.

The above considerations are not the only possible explanation for the 4500 cm^{-1} red shift of the computed emission band versus the experimental one, and probably cannot account for the whole of it.

Perhaps, the first option for an alternative explanation could be the effect of hydration. The presence of additional water molecules, possibly due to collisions of Al with water dimers, would produce a blue shift of the emission spectrum relative to that of the Al + H_2O reaction. As one can see in Figure 7, hydration brings M2 (i.e. the M2.nH_2O water adducts) very much below the energy level of Al + (n+1) H_2O and even Al + $(H_2O)_{n+1}$. However, under single collision conditions,[2] the partial pressure of water dimers is very low; for instance, for p_{H2O}=10^{-3} Torr, we should have approximately $p_{(H2O)2}$= $7\cdot10^{-11}$ Torr[40,41] for 300 K. Even if the reaction cross section for the Al-$(H_2O)_2$ interaction would be much larger than that of the Al-H_2O one, and the dynamics of the two-water system more complex than that of Al-H_2O, the water dimer pressure is probably too low. Besides, the $Al(H_2O)_{n+1}$ adducts might not react but dissociate, i.e. $Al(H_2O)_{n+1} \rightarrow Al(H_2O)_n + H_2O$ would be a competitive process.

Our computed *T*-averaged lifetimes for M2 are of the order of 600 fs, while the M2-H_2O collision frequency of one M2 molecule with H_2O would be approximately 10^4 s^{-1} for *T*=300 K (p_{H2O}=10^{-3} Torr and taking the collision diameter of *d*=3.2 Å). Excited M2 ($M2^*$) should be even less likely to undergo collisions. That lifetime value cannot be properly compared to former RRKM[8] or RRK[9] estimations because of the different conditions and because the system might not behave in an ergodic manner in such fast a process; still those estimations (0.1 ps[8] - 3 ps[9]) also point to a very fast frag-

mentation of M2. We cannot accurately compute the lifetime of M1 by the present computations; although for T=300 K we have estimated it to be of the order of 5 ps by RRKM theory,[8] while the M1-H_2O collision frequency would also be about 10^4 s^{-1} (300 K, 10^{-3} Torr and d=3.2 Å). These data show that the interaction of M1 or M2 with a further water molecule has a negligible probability.

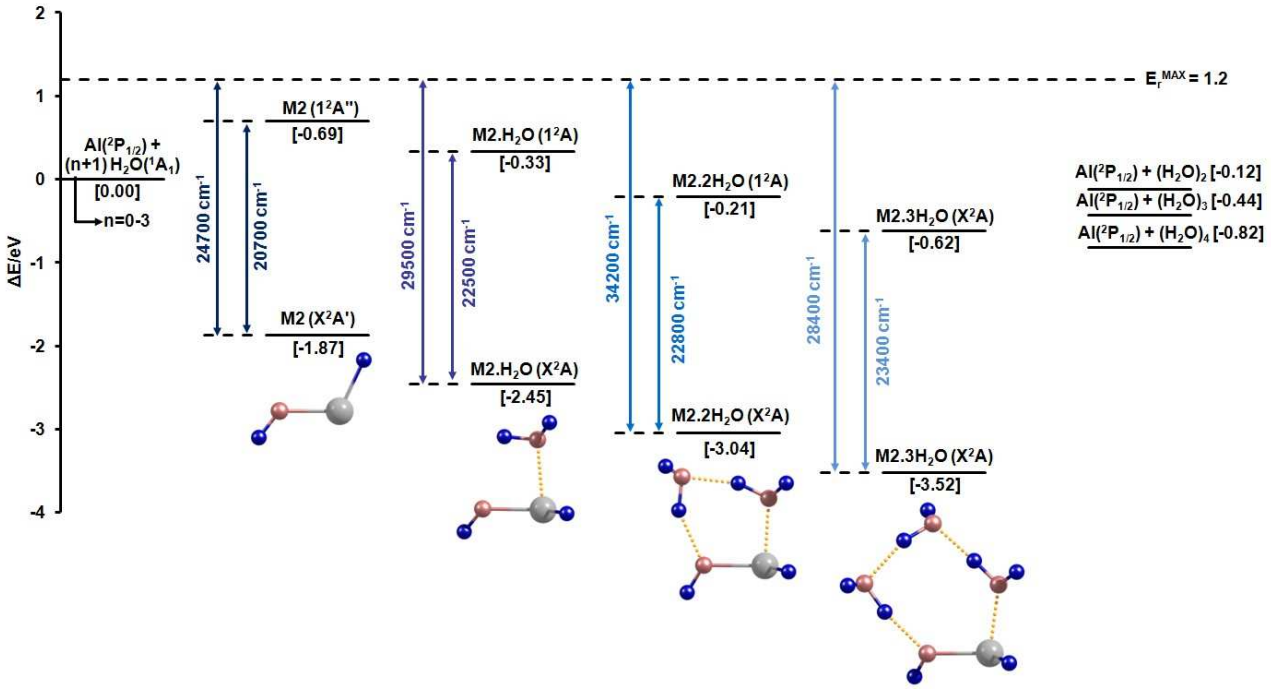

Figure 7. Representation of a possible origin of the short-wavelenght emission band. The maximum collision energy has been given a common value taken from the Al + H_2O collisions. The relative energies of ground state M2.n(H_2O) have been computed by the high-level procedure of ref 22, while the values of the corresponding first excited state have been computed by adding $T_{e,M2.nH2O}^{MRCI,corr} = T_{e,M2}^{MRCI} + \Delta T_{e,M2.nH2O}^{TD-DFT}$ with $\Delta T_{e,M2.nH2O}^{TD-DFT} = T_{e,M2.nH2O}^{TD-DFT} - T_{e,M2}^{TD-DFT}$, where $T_{e,M2}^{MRCI}$ is computed at the MRCI/aug-cc-pVTZ//QCISD/6-311++G(2df,p)[29,30,31,32] level and $T_{e,M2.nH2O}^{TD-DFT}$ is computed at the TD-BHandHLYP/aug-cc-pVTZ//BHandHLYP /aug-cc-pVTZ level.[42,30] The MRCI/aug-cc-pVTZ computations employ a CAS reference (ref 33), in which only the orbitals correlating to the 3d shell of Al are excluded.

The experimental spectrum shows that a small amount of aluminum atoms in the first excited ^2S state are present (emission doublet[43] at 25236 and 25348 cm^{-1}).While we could not explain presence of the Al(^2S) species in the beam (although one could think of some mechanism connected with the beam generation procedure), we performed preliminary calculations that showed the possibility of

an Al(^{2}S)-water exciplex with strong emission in the 35000-11500 cm^{-1} region. The radiative lifetime of Al(^{2}S) is 6.8 ns,[44] so only a very small fraction of it would undergo complex formation. Since the observed molecular emission is much stronger than the atomic one, we could, in principle, rule out this mechanism too. However, if there would be a mechanism for slow formation of the Al(^{2}S)-water exciplex, that emission could still be meaningful. The lowest quartet term, Al(^{4}P), is by 29020-29142 cm^{-1} above Al(X^{2}P$_{1/2}$) and would decay only very slowly to Al(X^{2}P) or Al(^{2}S); in other words, that quartet must be a long-lived species. The Al(^{4}P)-OH_2 interaction generates three PES (two of ^{4}A" symmetry and one of ^{4}A' symmetry for C_s geometries). Figure 8 presents two sets of energy profiles computed at the MRCI/aVTZ+Ry(2) level; they both employ structures optimized for a set fixed Al-O distances for the Al(^{2}S)-OH_2 state (first set) and for the $AlOH_2$(1^{4}A") state (second set). The basis set includes two shells of Rydberg-type functions (spd for Al and O[45]). The states which correlate with Al(X^{2}P/^{2}S/^{4}P)+OH_2 have been displayed. It is readily seen that the lowest quartet term is neatly attractive and even has a very short Al-O equilibrium distance, coming very close in energy to the Al(^{2}S)-OH_2 minimum in the second set of energy profiles. For decreasing Al-O distances the corresponding curves cross (as usual, the spin-orbit interaction is not taken into account), what means there could be a high probability of a spin-changing transition. The Al(^{2}S)-OH_2 complex formed in this way could decay by emission to the ground or the first excited state (high frequency) or to the dissociative 2^{2}A' state (low frequency). As said, the band caused by Al(^{2}S)-OH_2 could easily extend to frequencies higher than 25000 cm^{-1}. In other words we would have:

$$Al(^4P) + H_2O \Leftrightarrow AlOH_2(1^4A") \overset{ISC}{\rightarrow} Al(^2S)\text{-}OH_2 \rightarrow AlOH_2(X^2A") + h\nu$$

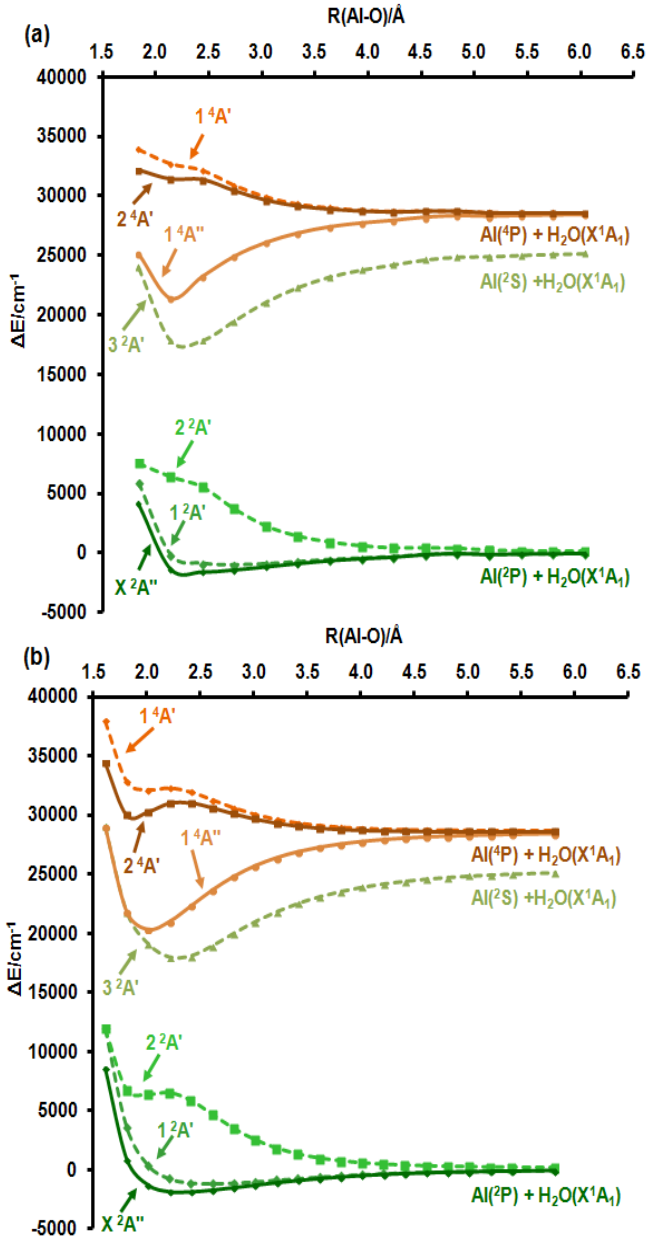

Figure 8. (a) MRCI/aVTZ+Ry(2) energy profiles computed of M1 as a function of the Al-O distance for the states which correlate with Al(^{2}P/^{2}S/^{4}P)-H_2O. The structures have been optimized for a set of fixed Al-O distances for the Al(^{2}S)-OH_2 state (3^2A') by TDDFT(BHHLYP)/6-311++G**+Ry(2) computations. (b) Same using BHHLYP/6-311++G** structures determined for the 1^4A" state. The energy gap between Al(^{2}P)-OH_2 and Al(^{4}P)-OH_2 has been computed at the CCSD(T)/aug-cc-pCVTZ level, correlating all electrons.

Where the emission could take place to the other two lower-lying doublets of M1 as well. By means of transition moment calculations we have verified that the Al(^{2}S)-OH_2 complex should emit at least as strongly as Al(^{2}S). Although dissociation (Al(^{2}S)-OH_2 → Al(^{2}S) + H_2O) could be a competing process, one cannot rule out that the dissociation time could be long enough as to allow emission to be a likely outcome. Note that both Al(^{2}S)-OH_2 and $AlOH_2$(1^4A"), contrary to $AlOH_2$(X^2A"), are rather deep minima on their respective PES; a long dissociation time is not impossible.

4. CONCLUSIONS

The high-temperature conditions of the oven where the Al beam is generated[1,2] should allow for a small population of the Al(^{4}P) term; at 1700 K, for instance, the equilibrium Al(^{4}P)/Al(X^2P) ratio should be ~$0.4x10^{-10}$. Even if that number is very small, it should be considered that the atomic Al(^{2}S) emission is clearly visible in the spectrum (the Al(^{2}S)/Al(X^2P) ratio would be $1.6x10^{-10}$) and also that, according to our TSH simulations, M2* accumulates emission probability during very short times (tens of fs). That means, in our view, that some contribution to the spectrum from the quartet term of Al through the exciplex formation process described above cannot be ruled out.

The collisions of Al atoms in a beam at 1700 K with water molecules in the gas phase produce a chemiluminescence due to an unknown species, previously hypothesized to be HAlOH.[1,2] In this work we investigate theoretically the collisions of Al atoms with water molecules. Surface hopping simulations with directly computed semiempirical PES confirm that the emitter can be HAlOH. This species is not formed directly in an excited state, which is instead populated by nonadiabatic

transitions from the hot ground state. The latter has a lifetime of about 0.6 ps, before dissociating to AlOH + H. Both the reaction and the total photo-emission cross sections are small ($6.3 \cdot 10^{-3}$ Å^2 and $2.7 \cdot 10^{-8}$ Å^2 respectively), therefore the simulation of the chemiluminescence spectrum required to run about $1.7 \cdot 10^5$ trajectories, a task that would not be easily performed by ab initio methods.

The computed spectrum exhibits two bands. One is in the near infrared, beyond the wavelength range experimentally investigated, and is due to an excited Al-H_2O complex. The other one is in the visible and is red shifted with respect to the experimental one, with two maxima at 15000 and 17500 cm^{-1}, instead of one at 22000 cm^{-1}. This is partly due to a small inaccuracy of the PES's in the region of the HAlOH minimum and perhaps also to artifacts of the surface hopping method. Other explanations of this discrepancy have been explored by accurate ab initio calculations, being beyond the scope of our simulations of the dynamics. One is the effect of interactions with more than one water molecule or reaction with water dimers, that would differently stabilize the ground and the excited state of the emitting species, causing a blue shift of the emission band. Another possibility is the formation of Al(^{4}P,^{2}S)-H_2O exciplexes, that would contribute to the short wavelength emission according to the computed potential energy curves. Both processes are far from being demonstrated, but they are worth further theoretical and experimental investigation.

ACKNOWLEDGMENT

SAB and JRF acknowledge the financial support of the Xunta de Galicia through the project IN-CITE09314252PR and the program IN845B-2010/036 and the services provided by the “Centro de Supercomputación de Galicia” (CESGA). SAB acknowledges a F.P.U. grant from the Spanish Ministry of Education. GG and MP acknowledge the financial support of the University of Pisa.

SUPPORTING INFORMATION AVAILABE:

Information about the reparametrization of the AM1 semiempirical method and about the analytical corrections (state-specific and geometry dependent corrections) applied. Data about the geometry of some minima and transition states are also included. This material is available free of charge via the Internet at http://pubs.acs.org.

REFERENCES:

[1] Oblath, S. B.; Gole, J. L. *J. Chem. Phys*. **1979**, *70*, 581-582

[2] Oblath, S. B.; Gole, J. L. *Combust. Flame* **1980**, *37*, 293-312

[3] Jones, M. R.; Brewster, M. Q. *J. Quant. Spectrosc. Radiat. Transfer.* **1991**, *46*, 109-118

[4] McClean, R. E.; Nelson, H. H.; Campbell, M. L. *J. Phys. Chem.* **1993**, *97*, 9673-9676

[5] Hauge, R. H.; Kauffman, J. W.; Margrave, J. L. *J. Am. Chem. Soc.* **1980**, *102*, 6005-6011

[6] Joly, H. A.; Howard, J. A.; Tomietto M.; Tse, J. S. *J. Chem. Soc., Faraday. Trans.* **1994**, *90*, 3145-3151

[7] Douglas, M. A.; Hauge, R. H.; Margrave, J. L. *J. Chem. Soc., Faraday Trans.* **1983**, *179*, 1533-1553

[8] Álvarez-Barcia, S.; Flores, J. R. *Chem. Phys.* **2011**, *382*, 92-97

[9] Shapirov, A.; Titova, N.; Starik, A. *J. Phys. Chem. A.* **2011**, *115*, 4476-4481

[10] Kurtz, H. A.; Jordan, K. D. *J. Am. Chem. Soc.* **1980**, *102*, 1177-1178.

[11] Sakai, S. *J. Phys. Chem.* **1992,** *96,* 8369-8373

[12] Sakai, S. *J. Phys. Chem.* **1993,** *97*, 8917-8921

[13] Jursic, B. S. *Chem. Phys.* **1998**, *237*, 51-58

[14] Watanabe, H.; Aoki, M.; Iwata, S. *Bull. Chem. Soc. Jpn*. **1993**, *66*, 3245-3252

[15] Sun, Y.-l.; Tian, Y.; Li, Shu-fen, *Ch. J. Chem. Phys.* **2008**, *21*, 245-249

[16] Agreiter, J. K.; Knight, A. M.; Duncan, M. A. *Chem. Phys. Lett.* **1999**, *313*, 162-170

[17] Álvarez-Barcia, S.; Flores, J. R. *Chem. Phys. Lett.* **2009**, *470*, 196-202

[18] Flores, J. R. *J. Chem. Phys.* **2006**, *125* 164309 (1-10)

[19] Flores, J. R. *Chem. Phys. Lett.* **1994**, *230* 358-364

[20] Tenebaum, E. D.; Ziurys, L. M. *Astrophys. J.* **2010**, *712*, L93-L96

[21] Álvarez-Barcia, S.; Flores, J. R. *Chem. Phys.* **2010**, *374*, 131-137

[22] Álvarez-Barcia, S.; Flores, J. R. *J. Chem. Phys.* **2009**, *131*, 174307 (1-11)

[23] Preuss, D. R.; Gole, J. L. *J. Chem. Phys.* **1977**, *66*, 2994-2999

[24] R. N. Porter and L. M. Raff, In *Dynamics of Molecular Collisions*, Part B; W. H. Miller, Ed.; Plenum Press: New York, **1976**; Chapter 1

[25] Granucci, G.; Persico, P.; Toniolo, A. *J. Chem. Phys.* **2001**, *114*, 10608-10615

[26] Ciminelli, C.; Granucci, G.; Persico, M. *J. Chem. Phys.* **2005**, *123*, 174317 (1-10)

[27] Dewar, M. J. S.; Zoebisch, E. G.; Healy, E. F.; Stewart, J. J. P. *J. Am. Chem. Soc.* **1985**, *107*, 3902-3909

[28] Cusati, T.; Granucci, G.; Martínez-Núñez, E.; Martini, F.; Persico, M.; Vázquez, S. *J. Phys. Chem. A* **2012**, *116*, 98-110

[29] Werner, H.-J.; Knowles, P. J. *J. Chem. Phys.* **1988**, *89*, 5803

[30] Dunning Jr.,T.H. *J. Chem. Phys.* **1989**, *90*, 1007-1023; Kendall, R. A; Dunning Jr.,T. H., Harrison, R. J. *J. Chem. Phys.* **1992**, *96*, 6796-6806; Woon, D. E. ;Dunning Jr.,T. H. *J. Chem. Phys.* **1993**, *98*, 1358-1371

[31] Pople, J. A.; Head-Gordon, M.; Raghavachari, K. *J. Chem. Phys.* **1987**, *87*, 5968-5975

[32] Frisch, M. J.; Pople, J. A.; Binkley, J. S. *J. Chem. Phys.* **1984**, *80*, 3265-3269

[33] Werner, H. -J.; Knowles, P. J. *J. Chem. Phys.* **1985**, *82*, 5053-5063

[34] McLean, A. D.; Chandler, G. S. *J. Chem. Phys.* **1980**, *72*, 5639-5648

[35] Clark, T.; Chandrasekhar, J.; Spitznagel, G. W.; Schleyer, P. v. R. *J. Comp. Chem*. **1983,** *4*, 294-301

[36] MOLPRO 2006 a package of *ab initio* programs, H.-J. Werner, P. J. Knowles, R. Lindh, F. R. Manby, M. Schütz, P. Celani, T. Korona, G. Rauhut, R. D. Amos, A. Bernhardsson, et al., see http://www.molpro.net .

[37] Tully, J. C. *J. Chem. Phys.* **1990**, *93*, 1061-1071

[38] Granucci,G; Persico, M. *J. Chem. Phys.* **2007,** *126*, 134114 (1-11)

[39] Stewart, J. J. P. MOPAC; Fujitsu Limited: Tokyo, Japan, **2002**

[40] Tretyakov, M. Y; Makarov, D; J. *Chem. Phys.* **2011**, *134*, 084306 (1-9)

[41] Scribano, Y.; Goldman, N.; Saykally, R. J.; Leforestier, C. *J. Phys. Chem. A* **2006**, *110*, 5411-5419

[42] Bauernschmitt, R.; Ahlrichs, R. *Chem. Phys. Lett.* **1996**, *256***,** 454-464

[43] Kaufman, V.; Martin, W. C. *J. Phys. Chem. Ref. Data* **1991**, *20*, 775-858

[44] Kelleher, D. E.; Podobedova, L. I. *J. Phys. Chem. Ref. Data* **2008**, *37*, 709-911

[45] Dunning Jr.,T. H.; Harrison, P. J., in *Modern Theoretical Chemistry,* VOL. 2. ED. H.F. Schaefer III, (Plenum, New York, **1977**).

SUPPLEMENTARY MATERIAL ACCOMPANIING THE MANUSCRIPT ENTITLED "A THEORETICAL STUDY OF THE CHEMILUMINESCENCE OF THE Al + H_2O REACTION" by Álvarez-Barcia et al.

Index

SM_T1. Original (AM1) and reaction-specific (AM1$^{(*)}$) parameters for the Al, O and H atoms. See MOPAC 2002 manual[a] for more details.

Parameter	AM1	AM1$^{(*)}$	Parameter	AM1	AM1$^{(*)}$
H			**Al**		
U_{SS}	-11.396427	-11.156258	U_{SS}	-24.353585	-24.990500
β_S	-6.173787	-6.605219	U_{PP}	-18.363645	-17.564669
ξ_S	1.188078	1.239553	β_S	-3.866822	-3.061546
α^a	*2.882324*	*2.882324*	β_P	-2.317146	-3.070327
G_{SS}	12.848000	14.577710	ξ_S	1.516593	1.442513
O			ξ_P	1.306347	1.298400
U_{SS}	-97.830000	-96.846787	α^a	1.976586	2.124841
U_{PP}	-78.262380	-72.477946	a_{kA}	0.090000	0.202711
β_S	-29.272773	-35.979391	b_{kA}	12.392443	1.973099
β_P	-29.272773	-27.032832	C_{kA}	2.050394	1.800000
ξ_S	3.108032	3.613391	G_{SS}	8.090000	7.973159
ξ_P	2.524039	2.265682	G_{SP}	6.630000	6.538902
α^a	*4.455371*	*4.455371*	G_{PP}	5.980000	8.462080
G_{SS}	15.420000	26.137650	G_{P2}	5.400000	5.274930
G_{SP}	14.480000	11.380641	H_{SP}	0.700000	0.803167
G_{PP}	14.520000	11.311851			
G_{P2}	12.980000	12.086095			
H_{SP}	3.940000	2.883505			

a) Stewart, J. J. P. MOPAC; Fujitsu Limited: Tokyo, Japan, **2002.** http://mtz01-a.stanford.edu/programs/documentation/mopac2002/index.html

b) The parameter α (repulsion "core"-"core") has been optimized, but only in case of Al.

Additive and multiplicative corrections to the potential energy surfaces.

The additive correction is the same for all electronic states and is a sum of terms:

$$U^{(add)} = \sum_{K=1}^{11} U_K^{(add)} \quad (1)$$

Each $U_K^{(add)}$ is associated with one of the internal coordinates: X_1= R(Al-O), X_2=R(Al-H_1), X_3=R(Al-H_2), X_4=R(O-H_1), X_5=R(O-H_2), X_6=R(H_1-H_2), X_7=cos(O-Al-H_1), X_8=cos(O-Al-H_2), X_9=cos(H_1-O-H_2), X_{10}=cos(Al-O-H_1) and X_{11}=cos(Al-O-H_2).

For K = 1, 4, 5 and 6 the additive contribution is

$$U_K^{(add)} = U_{K,S} + (U_{K,L} - U_{K,S})\ S(X_K, X_{K,S}, X_{K,L}) \quad (2)$$

where S is a cubic switching function defined as

$$\begin{aligned} S(X, X_S, X_L) &= 0 && \forall\, X \le X_S \\ S(X, X_S, X_L) &= 3\frac{(X - X_S)^2}{(X_L - X_S)^2} - 2\frac{(X - X_S)^3}{(X_L - X_S)^3} && \forall\, X_S \le X \le X_L \\ S(X, X_S, X_L) &= 1 && \forall\, X \ge X_L \end{aligned} \quad (3)$$

For K = *2* and *3* there is a damping factor depending on X_1:

$$U_K^{(add)} = U_{K,S} + (U_{K,L} - U_{K,S})\ S(X_K, X_{K,S}, X_{K,L})\ [1 - S(X_1, X_{D,S}, X_{D,L})] \quad (4)$$

For each angle A-B-C there are two damping factors, depending on X_A=R(A-B) and X_B=R(B-C):

$$\begin{aligned} U_K^{(add)} = {} & [U_{K,S} + (U_{K,L} - U_{K,S})\ S(X_K, X_{K,S}, X_{K,L})] \cdot \\ & \cdot [1 - S(X_A, X_{A,S}, X_{A,L})]\ [1 - S(X_B, X_{B,S}, X_{B,L})] \end{aligned} \quad (5)$$

The correction factors F_1 and F_2 multiply the energy difference between a state and the next one. More specifically, F_1 modifies the energy of the first excited state with respect to the ground state and F_2 modifies the energy of the second excited state with respect to the first one. General formulas are given in ref. 20. The F_1 factors depend on all six distances X_1-X_6 in the form of the product:

$$F_1 = \prod_{K=1}^{6} F_{1,K}(X_K) \quad (6)$$

with

$$F_{1,K}(X_K) = F_{1,K,S} + (F_{1,K,L} - F_{1,K,S})\ S(X_K, X_{K,S}, X_{K,L}) \quad (7)$$

Table SM_T2.
Parameters for the PESs corrections.
Distances in Å, angles in degrees and energies in eV.

Additive corrections (dependence on distances)									
K	X_K	$U_{K,S}$	$U_{K,L}$	$X_{K,S}$	$X_{K,L}$	$X_{D,S}$	$X_{D,L}$		
1	R(Al-O)	-0.028990	0.000000	1.60	2.30				
2, 3	R(Al-H)	-0.460324	0.000000	1.50	2.10	1.80	2.30		
4, 5	R(O-H)	-0.011495	0.000000	0.90	1.50				
6	R(H-H)	0.086554	0.000000	1.50	2.00				
Additive corrections (dependence on angles)									
K	X_K	$U_{K,S}$	$U_{K,L}$	$X_{K,S}$ [(a)]	$X_{K,L}$ [(a)]	$X_{A,S}$	$X_{A,L}$	$X_{B,S}$	$X_{B,L}$
7, 8	cos(O-Al-H)	0.607942	0.182039	180.0	120.0	1.60	2.30	1.50	2.10
9	cos(H-O-H)	0.354030	-0.110052	150.0	80.0	0.90	2.50	0.90	2.50
10,11	cos(Al-O-H)	0.098647	0.324410	180.0	10.0	1.60	2.30	0.90	1.50
Energy difference factors									
K	X_K	$F_{1,K,S}$	$F_{1,K,L}$	$F_{2,K,S}$	$F_{2,K,L}$				
1	R(Al-O)	0.638514	1.036990	0.724071	0.755195				
2, 3	R(Al-H)	1.047408	1.077875	1.258260	1.376547				
4, 5	R(O-H)	1.258799	1.020133	0.810797	0.941974				
6	R(H-H)	1.316743	1.039503	1.038310	1.050710				

[(a)] The lower and upper limits for the variation of the switching function are here given as angles (in degrees), but their cosines are used in the equation, consistently with the definition of the variables X_K.

SM_F1: Schematic representation of the most relevant minima and saddle points of the $AlOH_2$ system optimized at AM1(*)-FOMO-CI level. (The names in square brackets correspond to those of Figure 1 of the manuscript).[a]

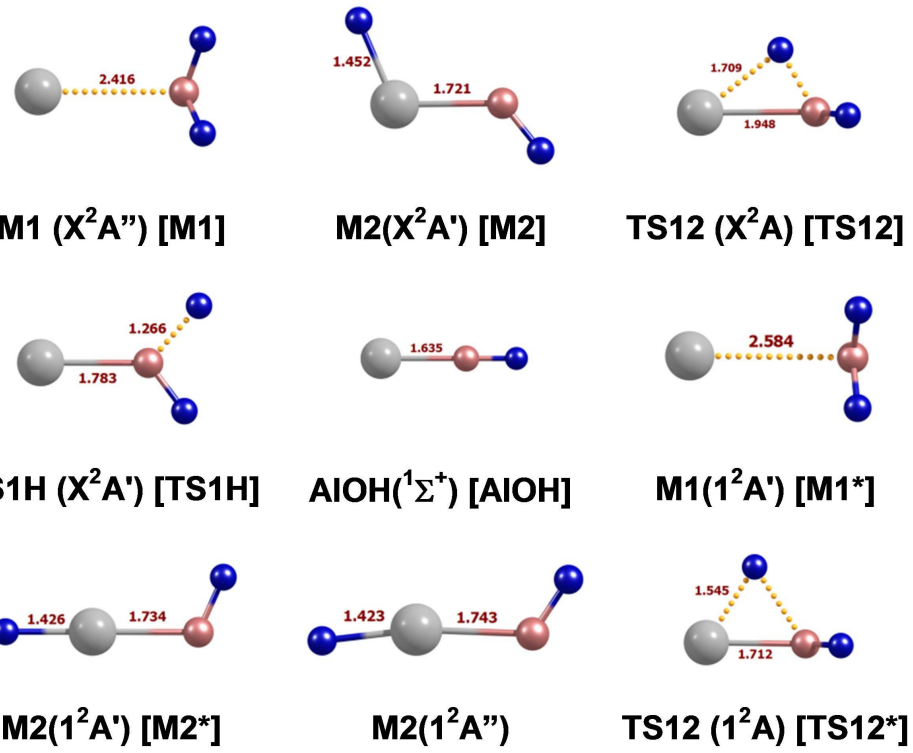

a. The M1(X^2A") state becomes X^2A' for planar C_s geometries.

SM_T3: Summary of the geometrical parameters (Å and °) of the optimized geometries for the most relevant minima and saddle points of the $AlOH_2$ system; the reference values are computed at the QCISD/6-311++G(2df,p) level for the ground state or the CASSCF/6-311++G** level for the excites states.

	AM1$^{(*)}$-FOMO-CI	Ref.	% error		AM1$^{(*)}$-FOMO-CI	Ref.	% error
Al+H_2O				**AlOH($^1\Sigma^+$) + H**			
R(O-H)	0.9872	0.9599	2.85	R(Al-O)	1.6349	1.6789	2.62
<(H-O-H)	103.97	104.90	0.88	R(O-H)	0.9628	0.9497	1.38
M1(X^2A")				<(Al-O-H)	180.04	180.00	0.02
R(Al-O)	2.4163	2.3016	4.99	**M1($1^2A'$)**			
R(O-H)	0.9955	0.9618	3.51	R(Al-O)	2.5842	2.7795	7.03
R(O-H)	0.9955	0.9618	3.51	R(O-H)	0.9944	0.9670	2.83
<(H-O-Al)	108.10	123.83	12.70	R(O-H)	0.9944	0.9670	2.83
<(H-O-H)	105.10	108.23	2.90	<(H-O-Al)	96.33	102.72	6.22
ϕ(H-O-H-Al)	115.3	157.9	26.98	<(H-O-Al)	96.33	102.72	6.22
M2(X^2A')				ϕ(H-O-Al-H)	103.2	110.9	6.92
R(Al-H)	1.4515	1.5947	8.98	**M2($1^2A'$)**			
R(Al-O)	1.7214	1.7068	0.86	R(Al-H)	1.4260	1.5805	9.78
R(O-H)	0.9703	0.9562	1.47	R(Al-O)	1.7341	1.7288	0.31
<(H-Al-O)	112.67	114.81	1.86	R(O-H)	0.9836	0.9633	2.11
<(Al-O-H)	128.13	125.11	2.42	<(H-Al-O)	179.79	180.75	0.53
ϕ(H-Al-O-H)	180.0	180.0	0.00	<(Al-O-H)	114.10	118.36	3.59
TS12(X^2A)				ϕ(H-Al-O-H)	140.04	180.00	22.20
R(O-H(Al))	1.2031	1.2619	4.66	**M2(1^2A")**			
R(Al-O)	1.9476	1.9117	1.88	R(Al-H)	1.4227	1.5781	9.84
R(O-H)	0.9904	0.9680	2.31	R(Al-O)	1.7427	1.6985	2.60
<(Al-O-H)	60.34	68.75	12.24	R(O-H)	0.9765	0.9526	2.51
<(H-O-Al)	128.27	128.01	0.20	<(H-Al-O)	171.20	170.97	0.14
ϕ(H-O-Al-H)	98.4	100.6	2.15	<(Al-O-H)	121.61	138.18	11.99
TS1H(X^2A')				ϕ(H-Al-O-H)	180.0	180.0	0.01
R(Al-O)	1.7825	1.8262	2.39	**TS12(1^2A)**			
R(O-H)	1.2657	1.2399	2.08	R(Al-O)	1.7116	1.8573	7.85
R(O-H)	0.9964	0.9702	2.70	R(O-H)	1.5925	1.5092	5.52
<(H-O-Al)	131.42	134.18	2.06	R(O-H)	1.0000	0.9735	2.71
<(H-O-Al)	127.00	121.97	4.13	<(H-O-Al)	55.62	60.97	8.78
ϕ(H-O-Al-H)	180.0	180.0	0.01	<(H-O-Al)	124.68	116.98	6.58
				ϕ(H-O-Al-H)	87.60	93.00	5.81

SM_T4: Description of the trajectory set; the number of trajectories per state, energy and impact parameter are given. Note that the final number includes the three different electronic states considered, which arise from Al(^{2}P).

E_R (eV)	b	N_{TRAJ}	# trajectories per E_R
0.00	B[a]	100	2100
0.10	B	100	2100
0.20	B_{TOT}[b]	100	3600
0.21-0.24; ΔE_R=0.01 (4)	B	100	8400
0.25	B_{TOT}	400	14400
0.26	B	100	2100
0.27	B	100	2100
0.275	B_{TOT}	400	14400
0.28	B	100	2100
0.29	B	100	2100
0.30	B_{TOT}	400	14400
0.31-0.34; ΔE_R=0.01 (4)	B	100	8400
0.35	B	400	8400
0.37	B	100	2100
0.40	B_{TOT}	400	14400
0.43	B	100	2100
0.45	B	400	8400
0.47	B	100	2100
0.50	B_{TOT}	100	3600
0.55	B	100	2100
0.60	B_{TOT}	100	3600
0.65-1.10; ΔE_R=0.05 (10)	B	100	21000
1.20-2.30; ΔE_R=0.10 (12)	B	100	25200
TOTAL			**169200**[c]

a) B=0.0, 0.5, 1.0, 1.5, 1.8, 2.0, 2.3 (Å)

b) $B_{TOT}=B + B_{INT} + B_{BIG}$

   (a) B_{INT} = 0.25, 0.75, 1.25 (Å)

   (b) B_{BIG} = 2.6, 2.8 (Å)

c) This is the total number or trajectories that we have been run, although among them there were 73 “bad” trajectories (discarded because of numerical faults and not considered in computing statistical results).